Performance Evaluation and Optimization of MIMO Radars Using Biomimetic Antenna Arrays

Ines Dorsch, Patrik Grüner, *Member, IEEE*, Markus Klose, David Schmucker, and Christian Waldschmidt, *Senior Member, IEEE*

Abstract— The improvement of the angular resolution of radar sensors is one of the crucial goals of current radar research. A promising approach to achieve this goal is inspired by the ears of a fly called *Ormia ochracea*. The working principle was adapted for antennas, and the so-called biomimetic antenna arrays (BMAAs) aroused the interest of several research groups. In this work, BMAAs are incorporated into multiple-input multiple-output (MIMO) arrays, a very common approach of improving the angular resolution, to gain more degrees of freedom in array design. The MIMO BMAAs are modeled utilizing the effective biomimetic antenna distance, a fundamentally new measure introduced in this article to translate the special biomimetic phase progression into a spatial quantity. We present straightforward antenna configurations but also describe how a genetic algorithm can be utilized to optimize both antenna positions and BMAA parameters. The proposed arrays show various beneficial effects such as a wider angular range for unambiguous angle estimation or a narrower beamwidth. The impact of MIMO BMAAs on the angular resolution is thoroughly analyzed both theoretically and by radar measurements in the range of 77 GHz. The measurements confirm the modeling method very well and show a significant increase in the angular separability.

Index Terms— Antenna arrays, biologically inspired antennas, biomimetic antenna arrays (BMAAs), direction-of-arrival (DOA) estimation, multiple-input multiple-output (MIMO), radar.

I. INTRODUCTION

RADAR sensors have become a standard sensor in both automotive and industrial applications, as they are insensitive to rough atmospheric conditions such as fog, dust, smoke, and occasional steam [1]. To get a better perception of the scene, additional angular information is needed besides the range and velocity information [2], [3]. In terms of angular resolution, radar lags behind lidar and camera and new approaches for improvement have to be found. Often, there are restrictions on the maximum size of the sensor, so multiple-input multiple-output (MIMO) radars are a popular measure to increase the antenna aperture virtually. Nevertheless, depending on the application and resulting restrictions,

compromises between the angular performance and the array size have to be made. In this article, we will introduce biomimetic coupling between receive (RX) antennas of MIMO arrays in order to gain further degrees of freedom in the design of the beam pattern (BP) and angular behavior of MIMO antenna arrays.

Conventional MIMO array setups using non-uniform spacing do not have a straightforward design rule, so the setup is often determined using a genetic algorithm with different possible optimization goals: low sidelobe levels [4], channel capacity for communication systems [5], minimum beamwidth/maximum aperture [6], or a maximum angular range for unambiguous angle estimation in the azimuth angular range [7] or in 2-D [8].

In this article, not only the MIMO principle is applied to enlarge the aperture but also the principle of biomimetic antenna arrays (BMAAs) is exploited. Such antenna arrays mimicking the hearing mechanism of the fly *Ormia ochracea* showed superior angle estimation behavior in various concepts [9], [10]. Advantages, among others, are a better angle estimation accuracy for arrays with fixed antenna spacing [11], [12], less required space for a predefined angular performance [13], or different possibilities to shape the BP of arrays [14], [15]. In contrast to the improvement of the angle estimation behavior through advanced signal processing, the processing time is not extended by BMAAs compared to conventional antennas using the same beamformer (usually a maximum likelihood estimator). Realizations of BMAAs can be found in the UHF band [16]–[19], around 20 GHz [11], 77 GHz [14], [20], 150 GHz [13], and 28.3 THz [21].

Other state-of-the-art BMAAs also use optimization processes, which differ in the optimization goal of this article. In [18] and [22], optimizers are used to determine admittance values for external coupling networks of closely spaced, mutually coupled antennas. The authors aim to achieve phase gain with maximized power extraction. Here, the biomimetic coupling mechanism is built up by a combination of an external biomimetic coupling network (BMC) and the antenna mutual coupling. In this work, it is not desirable to use BMCs depending on antenna mutual coupling. This would require closely spaced antennas and therefore restrict the possible antenna positions within the virtual aperture significantly. Using the model of [20], the antenna spacings can be chosen very flexibly and mutual antenna coupling does not have to be considered, which would be very challenging with regard to the operational frequency of 76.5 GHz. The disadvantage

is that enhancing the angular performance leads to a loss of output power, which is directly related to the degree of phase enhancement. Here, the optimization aims to find the optimum transmit (TX) and RX antenna positions and BMC parameters η, ξ to yield a larger ambiguity-free region (AFR) when compared to a MIMO array without biomimetic coupling using the same maximum space and number of antenna elements.

There are already concepts that combine the MIMO operation and BMAAs. In [17], the channel capacity of MIMO communication systems is enhanced using electrically small BMAAs at 615 MHz, [13] reduces the redundancy of two monostatic transmit–receive (TRX) antennas at 150 GHz, and [23] eliminates angular ambiguities resulting from restrictions of the monolithic microwave-integrated circuit (MMIC) positions of a 150-GHz 2-D imaging radar. In contrast to this work, these concepts use either very few antennas (1 TX and 2 RX in [17]) or are solely monostatic. Furthermore, a systematic, general approach for the array design is still missing.

Realized applications using BMAAs are HF localization for dense and indoor environments with closely spaced antennas [24], a compact extremely high frequency (EHF) radar-on-chip [13], and an infrared angle detector [21]. In general, the BMAA principle improves the angular sensitivity in a limited angular range for which, however, the output power is reduced. For this reason, applying biomimetic coupling is particularly suitable for near-field applications with a moderate angular range of interest.

This article presents for the first time that multistatic MIMO arrays benefit from multiple BMCs. Through this combination, the MIMO array design process gains significantly more degrees of freedom and leads to antenna arrays with considerably enhanced angular characteristics ranging from a wider AFR to locally increased angular resolution. The completely new concept of the effective biomimetic antenna distance is introduced as a simple, yet powerful, measure to account for the additional BMAA parameters in the MIMO BMAA design process. Straightforward, deterministic MIMO BMAAs, and genetically optimized designs are presented. Radar measurements verify both the modeling method and the superior angular characteristics of MIMO BMAAs. It is proven by measurements that MIMO BMAAs can enhance the angular resolution and, thus, the angular separability of two radar targets.

The article is structured as follows. Section II sums up the fundamentals of BMAAs and MIMO arrays. Section III explains the modeling, design, behavior, and advantages of MIMO BMAAs. In addition, Section III covers how MIMO BMAAs can be optimized using a genetic algorithm. Section IV describes optimized configurations and the manufactured antenna boards. In Section V radar measurements are presented.

II. FUNDAMENTALS

A. Two-Element BMAAs

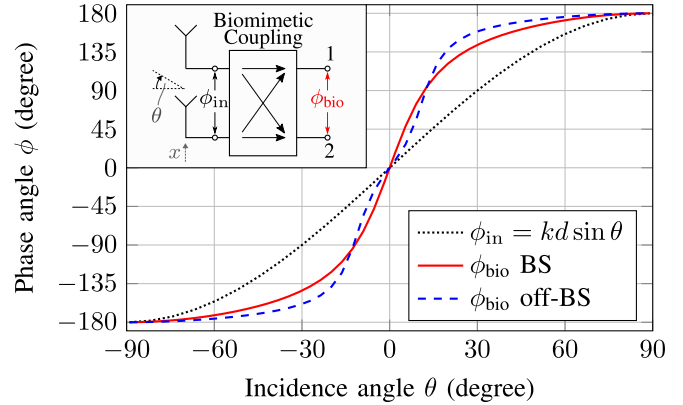The term BMAA in general refers to arrays exploiting biomimetic coupling following the example of the fly

Fig. 1. Biomimetic output phase progression ϕ_{bio} for a BS BMAA (——) and an off-BS BMAA (- - -) compared to the conventional phase progression (········) for the same antenna spacing $d = \lambda/2$ [13]. The BMAA parameters are $\eta = 3$, $\xi = 0$ (BS) and $\eta = 1.4$, $\xi = 2.5$ (off-BS).

Ormia ochracea. The first and still mostly used configuration consists of two biomimetically coupled antennas though more antennas and different types of coupling are possible [14], [22], [25], [26]. Thus, it must be explained for every design which array architecture is used. In this section, we describe the observable behavior of two biomimetically coupled antennas. The theory behind it and a comprehensive description of how the hearing system of the fly can be translated to a generalized model for electrical engineers are given in [20].

The conventional phase progression between two antennas is

$$\phi_{\mathrm{in}} = kd \sin \theta =: 2\alpha \qquad (1)$$

with $k = 2\pi/\lambda$ being the wavenumber, λ is the wavelength, d the physical distance between the antenna elements, θ is the angle of incidence of a plane wave, and α is an auxiliary parameter to simplify subsequent equations. A different behavior of the phase difference is obtained when introducing a BMC in between the two antennas, see the inset of Fig. 1. The output phase difference, called ϕ_{bio}, is considerably steeper around the boresight (BS) direction ($\theta = 0°$). In Fig. 1, two distinct biomimetic phase progressions are depicted. One ϕ_{bio} curve has its maximum steepness in BS direction (BS BMAA) and the other one shows two maxima of the slope lying symmetrically around BS (off-BS BMAA). The points of maximum slope indicate the incidence angle(s) with the maximum phase sensitivity. Two parameters determine which of the two characteristics is present for a BMAA: the phase gain η and the off-BS factor ξ. The phase gain is defined as the ratio

$$\eta = \left. \frac{d\phi_{\mathrm{bio}}(\theta)}{d\theta} \right|_{\theta=0°} \bigg/ \left. \frac{d\phi_{\mathrm{in}}(\theta)}{d\theta} \right|_{\theta=0°} \qquad (2)$$

representing the normalized slope of the biomimetic phase progression with respect to a conventional, uncoupled array of the same size in BS direction. The parameter ξ allows to yield off-BS behavior of the array when choosing $\xi > 0$. More precisely, the parameter ξ influences at which incidence angles $\pm\theta_0 \neq 0°$ the maximum phase slope is reached. For more information on off-BS BMAAs, see Table I and [27].

TABLE I
OVERVIEW OF TWO-ELEMENT BMAAs WITH ANTENNA
SPACINGS OF $d \leq \lambda/2$ [20], [27], [29]

	Conv.	BS BMAA	off-BS BMAA
ϕ_{bio}	ϕ_{in}	1 max of slope @$\theta = 0°$	2 max of slope @$\theta = \pm\theta_0$
L_{out}	0 dB	same @port 1, port 2 each 1 min @$\theta = 0°$	1 port min @$-\theta_0$ 1 port min @$+\theta_0$
η	1	> 1	
ξ	0	ideally: 0 generally: $|\xi| < |\eta|$	$|\xi| \gg |\eta|$

Although the biomimetic phase progression slope in Fig. 1 is increased around BS, it is decreased compared to the conventional phase progression slope for incidence angles $\theta \to \pm 90°$. This relation limits the operating angular range of every BMAA.

Using the generalized model of [20], which does not rely on mutual coupling of the antenna elements, the phase-amplifying mechanism comes with an inherent loss of output power. The output power of a BMAA with two antennas is always normalized to an identical array without biomimetic coupling [13], [28]

$$L_{\text{out}} = \frac{P_{\text{out,BMAA}}}{P_{\text{out,conv. Array}}} \tag{3}$$

$$= \frac{|1 \pm j(\eta + j\xi)\tan\alpha|^2}{|(\eta + j\xi) + j(\eta + j\xi)\tan\alpha|^2}. \tag{4}$$

The normalized output power L_{out} is always smaller than one. Table I gives an overview of the BMAA parameters, the resulting behavior for the two-element case with $d \leq \lambda/2$, and the respective parameters for a conventional antenna array. The biomimetic phase difference can be expressed as a function of the two parameters η and ξ [10]

$$\phi_{\text{bio}} = \arctan\left(\frac{2\eta\tan\alpha}{1 - (\eta^2 + \xi^2)\tan^2\alpha}\right). \tag{5}$$

The BMCs can be studied by either using the phenomenological description using the parameters d, η, and ξ or an equivalent circuit representation using an ideal transformer with the turning ratio $n = -1$, and a combination of resistors, inductors, and capacitors (see [20]).

B. MIMO Arrays and Signal Model

The signal model in this article is similar to [13], [30]. Several TX ($p = 1, \ldots, M_t$) and RX antennas ($q = 1, \ldots, M_r$) are considered and lie on the x-axis. As only linear arrays are analyzed in this work, only one angular domain, the azimuth plane with the angle θ, is of interest (cf., inset Fig. 1). All targets are assumed to be in the far-field and an antenna is either a TX or an RX antenna (multistatic operation). To achieve a MIMO operation, the TX signals have to be orthogonal, which can be ensured by any multiplexing scheme. The TX- and RX-steering vectors can be defined in dependence of the positions of the TX antennas x_{tp} and

of the RX antennas x_{rq}

$$\mathbf{a}_{\text{TX}}(\theta) = \begin{pmatrix} e^{jkx_{t1}\sin\theta} \\ \vdots \\ e^{jkx_{tM_t}\sin\theta} \end{pmatrix}, \quad \mathbf{a}_{\text{RX}}(\theta) = \begin{pmatrix} e^{jkx_{r1}\sin\theta} \\ \vdots \\ e^{jkx_{rM_r}\sin\theta} \end{pmatrix} \tag{6}$$

As a consequence of the orthogonality of the TX signals, a virtual aperture can be set up with a virtual steering vector defined as

$$\mathbf{a}(\theta) = \mathbf{a}_{\text{TX}}(\theta) \otimes \mathbf{a}_{\text{RX}}(\theta) = \begin{pmatrix} e^{jkx_{v1}\sin\theta} \\ \vdots \\ e^{jkx_{v(M_t M_r)}\sin\theta} \end{pmatrix}. \tag{7}$$

Here, $\otimes$ denotes the Kronecker product. The resulting vector contains the virtual antenna positions x_v having the dimension $(M_t M_r \times 1)$. The ambiguity function (AF) of the MIMO configuration is a useful quantity when analyzing the angular performance of the antenna setup and is defined as [31]

$$\text{AF}(\theta_i, \theta_j) = \frac{|\mathbf{a}(\theta_i)^H \cdot \mathbf{a}(\theta_j)|}{\|\mathbf{a}(\theta_i)\| \|\mathbf{a}(\theta_j)\|} \tag{8}$$

using the Hermitian operator $(\cdot)^H$ and the Euclidean norm of a vector $\|\cdot\|$. The AF may be regarded as a correlation of the steering vector with itself and, thus, equals values between 0 and 1, where 1 corresponds to maximum resemblance. Ideally, only angles $\theta_i = \theta_j$ yield maximum resemblance as high values for $\theta_i \neq \theta_j$ indicate ambiguities in the angle estimation. When all TX and RX antennas are identical, the properties of the AF are independent of the complex radiation pattern and only affected by the antenna placement [30]. The AFR is a frequently used metric to compare the angular performance of several antenna arrays in terms of ambiguities. The AFR is defined by the biggest possible square region of the AF centered around BS, which can be drawn without exceeding a defined auto-correlation threshold value. Unless otherwise stated, the threshold is 0.5 in this article. Furthermore, the virtual antenna steering vector can be used to analyze the angular resolution of the array configuration. The transmit–receive BP at the steering angle θ_0 is defined as [32]

$$\text{BP}(\theta, \theta_0) = \frac{|\mathbf{a}(\theta)^H \cdot \mathbf{a}(\theta_0)|^2}{\|\mathbf{a}(\theta)\|^2}. \tag{9}$$

III. DESIGN OF BIOMIMETIC MIMO ARRAYS

This section first answers the question of how to model BMAAs as part of the virtual aperture of a MIMO radar system. Next, we describe how we incorporated BMAAs in MIMO arrays and how this combination impacts the angular domain.

A. Modeling of MIMO BMAAs Using the Effective Biomimetic Antenna Distance

Usually, when talking about BMAAs the biomimetic phase progression ϕ_{bio} and the normalized output power at the antenna ports L_{out} are being investigated, cf., Section II. Conventional MIMO antenna array configurations with multiple TX and RX antennas usually consider the relative antenna

positions instead of the phase progressions. The antenna positions are then used to build up the virtual aperture containing all MIMO channels [cf., (6) and (7)].

Analogous to the classical MIMO approach, it is advantageous to model the behavior of BMAAs in terms of antenna positions. To do so, we consider Fig. 1. Using conventional, uncoupled antennas, the output phase difference of the antenna array corresponds to the input phase progression $\phi_{\text{in}} = kd \sin \theta$ as the biomimetic coupling is absent, cf., Fig. 1. For BMAAs with an antenna spacing of $d \leq \lambda/2$, it can be seen from Fig. 1 that the absolute value of the biomimetic output phase progression ϕ_{bio} exceeds or equals the conventional phase progression ϕ_{in} for every incidence angle $-90° \leq \theta \leq 90°$, that is

$$|\phi_{\text{bio}}| \geq |\phi_{\text{in}}| = |kd \sin \theta|, \quad d \leq \lambda/2. \tag{10}$$

For a fixed incidence angle $\theta = \theta_0$, this corresponds to a greater phase difference between the output ports of the biomimetic coupling than the physical aperture can yield

$$|\phi_{\text{bio}}| = |\tilde{k}\tilde{d} \sin \theta_0| \geq |kd \sin \theta_0|. \tag{11}$$

The wavenumber k is a quantity determined by the operating frequency of the radar system used and the factor $\sin \theta$ follows from trigonometry. Both are not affected by the biomimetic coupling, so $\tilde{k} = k$. Hence, the greater biomimetic output phase in (11) can be translated to an antenna distance greater than the physical antenna distance $\tilde{d} > d$. In the following, this greater antenna distance seen at the outputs is called effective biomimetic antenna distance d_{bio}. As $\phi_{\text{bio}} = \phi_{\text{bio}}(\theta)$ is a function of the incidence angle θ, so is $d_{\text{bio}} = d_{\text{bio}}(\theta)$. The inequality (10) can thus be rewritten as

$$|\phi_{\text{bio}}| = |kd_{\text{bio}}(\theta) \sin \theta| \geq |\phi_{\text{in}}| = |kd \sin \theta|. \tag{12}$$

The effective biomimetic antenna distance can be calculated with the help of (5) to

$$d_{\text{bio}}(\theta) = \frac{\phi_{\text{bio}}(\theta)}{k \sin \theta} \tag{13}$$

$$= \frac{\arctan\left(\dfrac{2\eta \tan \alpha}{1 - (\eta^2 + \xi^2) \tan^2 \alpha}\right)}{k \sin \theta}. \tag{14}$$

With L'Hôpital's rule it can be shown that

$$\lim_{\theta \to \pm 0°} d_{\text{bio}}(\theta) = \eta d. \tag{15}$$

This means that in BS direction the antenna distance between two biomimetically coupled antennas seems to be larger by the factor of the phase gain η compared to two conventional antennas separated by the antenna distance d. The quantity $d_{\text{bio}}(\theta)$ is angle dependent, always greater than the physical antenna distance d for $d \leq \lambda/2$ and only an equivalent quantity expressing the difference in phase between the BMAA and a conventional two-element array. $d_{\text{bio}}(\theta)$ is always centered around the midpoint between the two biomimetically coupled antennas. Two examples for $d_{\text{bio}}(\theta)$ are depicted in Fig. 2, where $d_{\text{bio}}(\theta)$ is normalized to the physical antenna spacing d. The maximum/maxima of $d_{\text{bio}}(\theta)$ correspond(s) to the incidence angle(s) θ, where the biomimetic
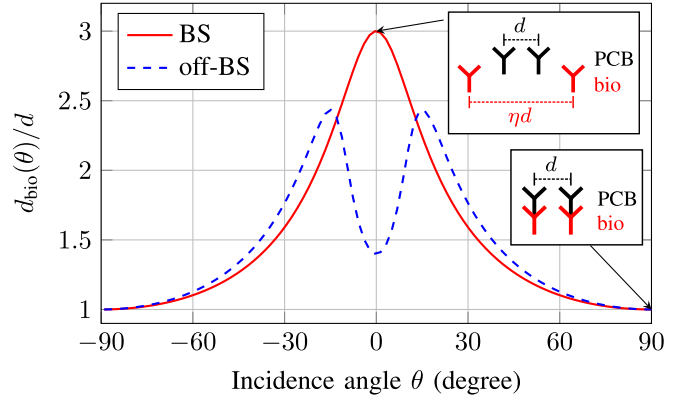

Fig. 2. Angle-dependent, effective biomimetic antenna distance $d_{\text{bio}}(\theta)$ relative to the physical antenna spacing (here: $d = \lambda/2$). The BMAA parameters are identical to the ones in Fig. 1. The insets demonstrate what antenna spacing the biomimetically coupled antennas seem to have (red antennas) compared to the antenna spacing on the PCB (black antennas) for the BS BMAA.

output phase progression ϕ_{bio} has its maximum steepness. So, for a BS BMAA (cf., Table I), $d_{\text{bio}}(\theta)$ reaches its maximum at $\theta = 0°$, whereas it shows two maxima for an off-BS configuration. The course of $d_{\text{bio}}(\theta)$ is always symmetrical to $\theta = 0°$. As $\phi_{\text{bio}}(\theta)$ in Fig. 1 approaches the phase progression for the conventional array for $\theta \to \pm 90°$, $d_{\text{bio}}(\theta)$ converges to the physical antenna distance d (see Fig. 2). Using d_{bio}, it is now possible to translate the characteristic biomimetic phase progressions to equivalent, angle-dependent antenna positions.

If two antennas having a larger physical antenna spacing than $\lambda/2$ are biomimetically coupled, the biomimetic phase difference does not exceed the conventional phase progression for all angles θ, see Fig. 3(a). Instead, ϕ_{bio} meanders around the reference curve. This behavior results in an effective biomimetic antenna distance d$_{\text{bio}}$, which is not always greater than d. Consequently, this limits the interesting angular range ($d_{\text{bio}} > d$), which is, in this example, mainly pronounced around the BS direction [here: $|\theta| \leq 19.5°$, see Fig. 3(b)]. Thus, the biomimetic effect is more impactful for a wider angular range if moderate physical antenna spacings d are chosen in between the biomimetically coupled antennas (cf., Fig. 2).

B. Design of MIMO BMAAs

In this section, we describe the effects on the virtual aperture, when BMAAs are part of a MIMO antenna setup. In this work, only pairs of RX antennas are biomimetically coupled. Utilizing BMAAs with more than two biomimetically coupled antennas would make it more difficult to understand the basic concept, whereas the observable effects are identical [14]. All RX and TX antenna elements are of the same type. However, the TX antennas of the MIMO array configuration are not connected to BMCs and therefore behave like conventional antennas.

1) Deterministic Biomimetic MIMO Array Design: In this context deterministic means that the array configurations covered in this section are chosen by hand and no optimization process has taken place. The antenna positions and BMAA
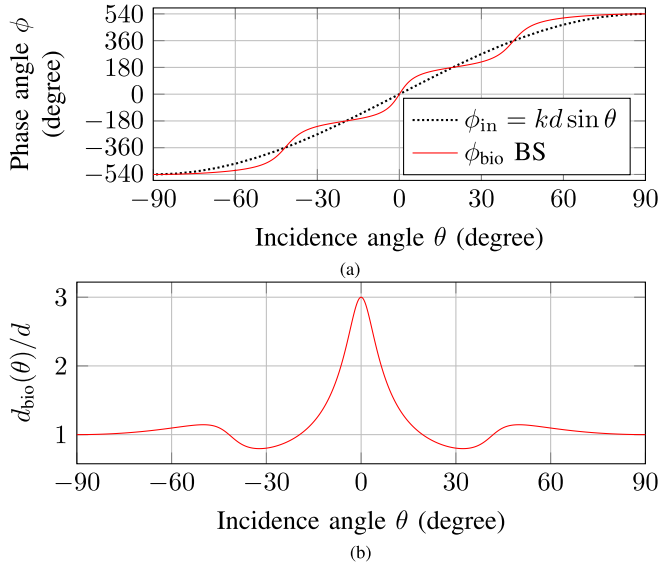
Fig. 3. (a) Exemplary phase progression and (b) normalized effective biomimetic antenna distance $d_{\mathrm{bio}}(\theta)$ for a BS BMAA with physical antenna spacing $d > \lambda/2$. Specific parameters: $\eta = 3$, $\xi = 0$, and $d = 1.5\lambda$.

TABLE II
ANTENNA PARAMETERS OF LAYOUTS IN SECTION III-B

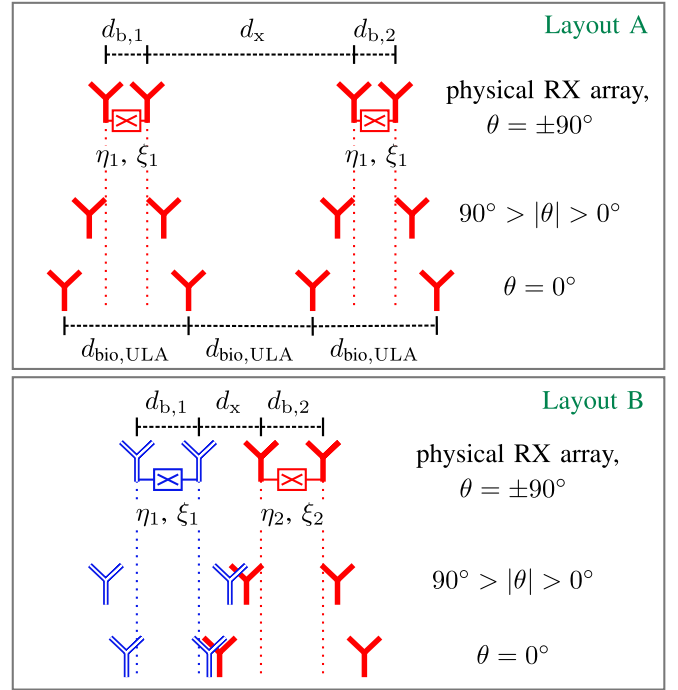|			Layout A	Layout B
TX	Positions		4-element ULA with $d_{\mathrm{TX}} > d_{\mathrm{RX,tot}}$	4-element ULA with $d_{\mathrm{TX}} \approx d_{\mathrm{x}}$
RX	Positions		$d_{\mathrm{b},1} = d_{\mathrm{b},2}$ $d_{\mathrm{x}} \gg d_{\mathrm{b},1}$	$d_{\mathrm{b},1} = d_{\mathrm{b},2} = d_{\mathrm{x}}$ $d_{\mathrm{x}} = \lambda/2$
	BMAA Par.	η_1	> 1	≥ 1
		ξ_1	0	$\gg \eta_1$
		η_2	η_1	> 1
		ξ_2	ξ_1	0

Fig. 4. Two exemplary layouts of four-element RX arrays utilizing BMAAs as part of the array. The effective biomimetic aperture is identical to the physical aperture on the PCB for $\theta = \pm90°$ for both layouts, because $d_{b,1} = d_{b,2} = \lambda/2$ is chosen here. Below the physical RX array, it can be seen how $d_{\mathrm{bio}}(\theta)$ influences the RX aperture. Antennas of BS BMAAs are drawn red filled, antennas of off-BS BMAAs blue striped.

parameters are selected in such a way that the effects on the RX aperture can be demonstrated in a descriptive manner. Fig. 4 depicts two layouts with four RX antennas that are biomimetically coupled in pairs. The two BMAA pairs are separated by a distance of d_x, whereas the antenna spacings within one BMAA pair are $d_{b,1}$ and $d_{b,2}$, respectively. In Layout A, the BMAA parameters are chosen to be equal and they show a BS characteristic with $\eta_1 = \eta_2 > 1$ and $\xi_1 = \xi_2 = 0$ (cf., Table I). The conditions for the two examples of Fig. 4 are also listed in Table II. In this example, d_x is significantly larger than the antenna spacings of the two BMAA pairs, which are chosen to be identical ($d_{b,1} = d_{b,2}$). This corresponds to an example where great sparsity is present and antenna elements cannot be distributed evenly, e.g., because of space limitations on the printed circuit board (PCB). Fig. 4 also presents the equivalent RX antenna positions, which are angle-dependent because of the presence of BMCs. For target angles $\theta \approx \pm90°$, in Fig. 4, the effective biomimetic antenna distances are small and for $d_{b,1} = d_{b,2} = \lambda/2$ identical to the physical aperture. The sparsity is still present. We now consider a radar point target that is moving on a circular path around the array toward BS [changing direction-of-arrival (DOA) but fixed range]. As the

target approaches the BS direction ($|\theta| \to 0°$), the effective biomimetic antenna distances become greater than the physical antenna spacings of the BMAA pairs $d_{b,1} = d_{b,2}$ (cf., Section III-A). The biomimetically coupled antennas seem to move away from each other with respect to their center. Because both BMAA pairs in Layout A have the same biomimetic characteristic, this applies for both BMAA pairs. The BMAAs reach their maximum $d_{\mathrm{bio}}(\theta)$ in this example for targets in BS direction. For this angle, the aperture seen is maximized and the large gap in between the two BMAA pairs (d_x on the PCB) has become smaller. An effective uniform linear array (ULA) with antenna spacings of $d_{\mathrm{bio,ULA}}$ may result in BS direction, when choosing the antenna parameters $d_x, d_{b,1}, d_{b,2}, \eta_1, \eta_2, \xi_1$, and ξ_2 properly. This is depicted at the bottom of Layout A in Fig. 4. As a consequence of the biomimetically coupled RX antennas, which seem to move depending on the incidence angle θ, the vector containing the RX antenna positions becomes a function of the incidence angle: $\boldsymbol{x}_r(\theta)$. Accordingly, the positions of the virtual antennas [see (7)] are also angle-dependent: $\boldsymbol{x}_v(\theta)$.

Fig. 5 shows the AF of a virtual array corresponding to Layout A. Here, the TX antennas are organized as an ULA with an antenna spacing of d_{TX}, which is bigger than the total RX aperture on the PCB $d_{\mathrm{RX,tot}} = d_{b,1} + d_x + d_{b,2}$. The antenna parameters in Fig. 5 are chosen as described in Table III, Layout A. Fig. 5(a) shows the AF with the biomimetically coupled RX antennas. Fig. 5(b) and (c) serve for comparison. Fig. 5(c) shows the AF of the virtual aperture using only conventional, not biomimetically coupled antennas at the same
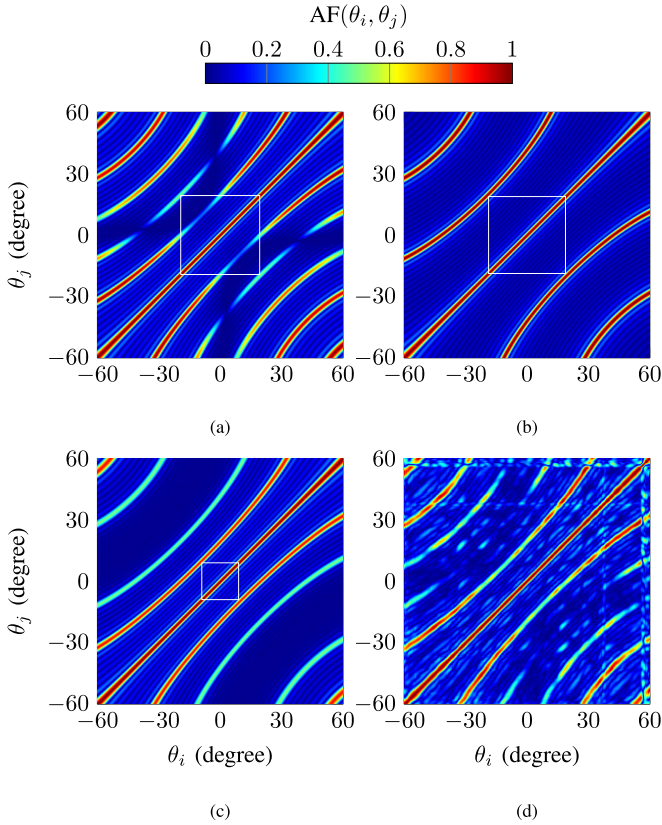
Fig. 5. (a) AF for a MIMO BMAA according to Layout A in Fig. 4 and Table III (AFR $= -19.3°, \ldots, 19.3°$). (b) AF of an array with the same aperture as Layout A in BS direction (AFR $= -18.8°, \ldots, 18.8°$). (c) Corresponds to the AF of the physical aperture on the PCB without BMCs (AFR $= -9°, \ldots, 9°$). The rectangles indicate the AFRs of the configurations. (d) Shows the measurement of (a) presented in Section V.
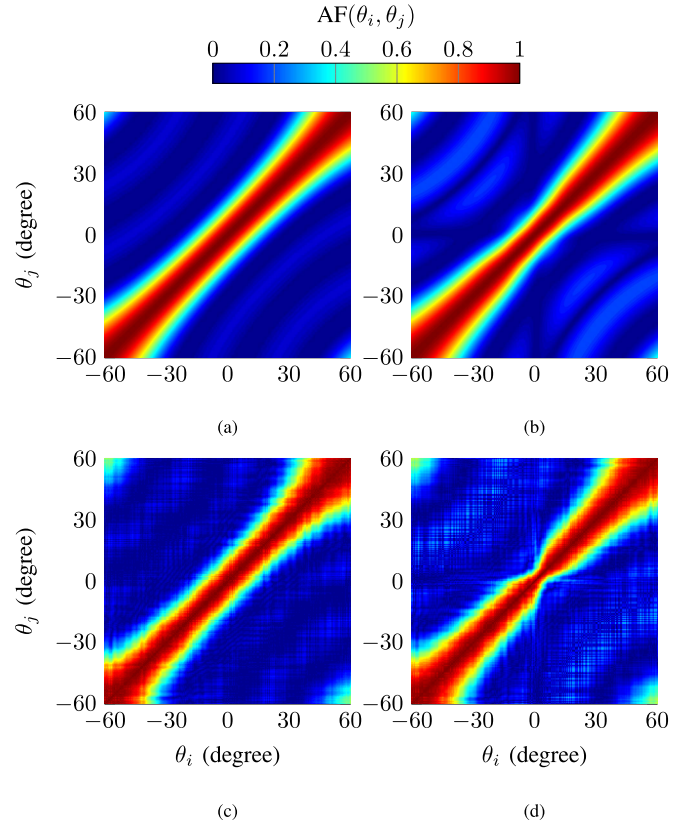

Fig. 6. (a) Simulated and (c) measured (see Section V) AF of the virtual array build up by two four-element ULAs (TX and RX) with an antenna spacing of $d = (\lambda/2)$. The AF for the same antenna placement utilizing BMAAs in the RX array corresponding to Layout B in Fig. 4 and Table II is shown in (b) through simulation and (d) through measurement. The array parameters are selected identical to the ones of Table III (second column).

positions as in Fig. 5(a). Fig. 5(b) depicts the AF of a virtual array, which has fixed (angle-independent) antenna positions at the same positions as it is seen by the biomimetic array of Layout A in BS direction. In this example, the TX locations are identical, but the RX array is a four-element ULA with an antenna spacing of $d_{\mathrm{bio,ULA}} = \eta_1 \, d_{b,1} = 3(0.5\lambda) = 1.5\lambda$. This means the RX array of Fig. 5(b) is physically larger than the one of Fig. 5(a).

Both the equivalent BS array of Fig. 5(b) and the physical virtual array of Fig. 5(c) show ambiguities in the depicted angular range and a limited AFR. However, it can be seen that the biomimetic AF of Fig. 5(a) can be regarded as a combination or overlay of the two array configurations in Fig. 5(b) and (c). Also, the AFR of the biomimetic MIMO array of Fig. 5(a) of $-19.3°, \ldots, 19.3°$ is significantly enlarged compared to Fig. 5(c) with an AFR of $9°$ even though the antenna elements are placed at the exact same positions on the PCB. The AFR of the biomimetic antenna configuration is even bigger than the one of the equivalent array in BS direction (AFR $= -18.8°, \ldots, 18.8°$). This is because the magnitude of the first ambiguities of Fig. 5(b) is reduced as the equivalent RX array is in transition between the effective biomimetic RX positions in BS direction [Fig. 5(b)] and the physical configuration on the PCB [Fig. 5(c)]. Fig. 5(d) depicts the corresponding measurement to Fig. 5(a) and confirms the simulation very well. A more detailed description of the measurement setup and the results follow in Section V. The

normalized output power L_{out} of the two BMAAs has a minimum value of $L_{\mathrm{out,min}} = -9.5$ dB at BS.

In the second example of Fig. 4, Layout B, four RX antennas are considered in an ULA placement with an antenna spacing of $d_{b,1} = d_{b,2} = d_x$. The TX array is a four-element ULA with an antenna spacing similar to that of the RX array, see Table II. In this layout, two distinct BMAA configurations are considered for the two BMAA pairs: one BS BMAA (drawn in red) and one off-BS BMAA (blue) according to Table I. The BS BMAA reaches its maximum effective aperture for $\theta = 0°$, whereas the off-BS BMAA has its maximum extend at $90° > |\theta| > 0°$. Combining these two BMAA configurations leads to a significantly larger aperture for an extended angular range around BS, as can be seen in Fig. 4.

In Fig. 6 an AF using Layout B as RX antenna setup is depicted. Again, the specific antenna parameters can be found in Table III. Compared to the AF of the virtual array of the physical aperture on the PCB [Fig. 6(a)], the width of the diagonal ($\theta_i = \theta_j$) is narrower for the biomimetic MIMO array in the range of $\theta = -20°, \ldots, 20°$ in Fig. 6(b). This indicates a smaller beamwidth (BW) of the main beam according to (9) and therefore, the resolution is improved in this angular range by applying biomimetically coupled antennas. The minimum normalized output power levels are $L_{\mathrm{out,min}} = -12.7$ dB for the BS BMAA and $L_{\mathrm{out,min}} = -15.8$ dB at $\theta = \pm 11°$ for the off-BS BMAA.

TABLE III
DETERMINISTIC CONFIGURATIONS OF MIMO BMAAS AT 76.5 GHz

			BMAA larger AFR cf. Layout A	BMAA smaller BW cf. Layout B
TX	Positions		$(0, 6, 12, 18)\lambda$	$(0, 0.5, 1, 1.5)\lambda$
	Positions		$(0, 0.5, 3, 3.5)\lambda$	$(0, 0.5, 1, 1.5)\lambda$
RX	BMAA Par.	η_1	3	1.4
		ξ_1	0	2.5
		η_2	3	4.3
		ξ_2	0	0

2) Optimization of Antenna Parameters by a Genetic Algorithm: In Section III-B.1 it was shown that two effects can be observed when using BMAAs as part of the RX array for MIMO antenna arrays. First, the AFR of a MIMO antenna array can be enlarged significantly when the placement of the antennas shows large sparsity leading to ambiguities. Second, BMAAs in a MIMO antenna array can achieve an effective aperture, which is seen bigger than the aperture resulting from the physical positions of the antennas on the PCB. Thus, the BW is reduced and the angular resolution is enhanced. Apart from that more yieldable effects are possible. A MIMO BMAA can have a comparable AFR but lower limiting grating lobe levels (lobes above a defined AF threshold limiting the AFR) compared to an uncoupled MIMO array. And MIMO BMAAs with an equivalent AFR but lower sidelobe levels (lobes below a defined AF threshold not limiting the AFR) are possible.

So far, the presented antenna array configurations were chosen by hand to show some of the observable effects. In this section, antenna parameters will be optimized using a genetic algorithm. A population of chromosomes evolves over multiple iterations, also called generations. The chromosomes consist of genes that represent the parameters we strive to optimize. For a flowchart and more detailed explanations on the theory of the genetic algorithm, we refer to [33], [34]. In this work, the structure of the biological hierarchy is as follows.

1) Ten genes form one chromosome: two genes representing the positions of two TX antennas, two genes represent the center positions of two pairs of BMAAs forming the RX array, four genes for the BMAA parameters (η_1, ξ_1, η_2, ξ_2) and two genes for the physical antenna spacing of the two BMAA pairs.

2) 40 chromosomes, each representing one MIMO BMAA configuration, form one generation, also called a population.

3) New generations are formed until all conditions are met or a maximum number of iterations $N_{\text{iter,max}}$ is reached.

4) Multiple runs, defined by N_{runs}, are performed optimizing independent initial populations. This reduces the chances to receive a local optimization maximum in contrast to a global optimization maximum.

To obtain physically feasible and reasonable solutions, the following restrictions and variables were set.

1) Maximum widths of the TX and the RX array $w_{\text{TX,max}}$ and $w_{\text{RX,max}}$ are set.

2) A range for the allowed spacings between the antennas forming the BMAA pairs is specified: $d_{b,x} = \lambda/2, \ldots, d_{b,\text{max}}$.

3) Possible antenna positions are defined by a grid of size 0.5 mm.

4) The effective biomimetic antenna positions within the virtual array shall not cross.

5) All antenna elements on the PCB should have a minimum distance of $\lambda/2$ to one another to avoid mutual coupling between the antenna elements.

6) The virtual aperture resulting from the physical positions of the antennas (effect of effective biomimetic antenna distance neglected) should be greater than or equal to $w_{\text{VX,min}}$.

7) The BMAA parameters η and ξ are limited to $\eta = 1, \ldots, \eta_{\text{max}}, \xi = 0, \ldots, \xi_{\text{max}}$ with a step size of 0.1.

8) A threshold for ambiguities is set by the variable $\text{AF}_{\text{threshold}}$.

In case a chromosome contradicts one of these restrictions its rating, i.e., the fitness, is set to zero. Beyond that, the fitness is evaluated based on the AFR of the virtual array. A configuration showing a larger AFR is rated with a higher fitness value. Adding the normalized output power of the channels L_{out} (also limiting the BMAA parameters) or the resulting BW at an angle θ of interest to the fitness function is also imaginable but was not used for optimization in this work. The initial population is generated by randomly choosing values out of the parameter alphabets. For every newly created generation the fitness function is evaluated. Next, the selection of chromosomes for the mating pool for further generations is conducted in a rank-based manner. After (uniform) recombination of the chromosomes within the mating pool, mutation and elitism are utilized before the fitness of all chromosomes is calculated again. These steps are performed for every generation until a desired AFR is obtained or the maximum number of passes $N_{\text{iter,max}}$ is reached. The whole procedure is repeated N_{runs} times. The chromosome with the highest fitness of all runs is the antenna configuration, which was optimized best.

To be able to draw a fair comparison to MIMO BMAAs, two configurations serve as comparisons: on the one hand, we compare the optimized MIMO BMAA configurations found by the genetic algorithm with an antenna board having antennas at the same physical positions but without the insertion of BMCs. On the other hand, we use the genetic algorithm to optimize a MIMO antenna array without biomimetic coupling applied. For the latter, the same restrictions concerning the number of antennas, antenna positions, and PCB area apply as for the biomimetic optimization. But the number of genes within this optimization differs from the genetic optimization for MIMO BMAAs. A chromosome consists of only six genes: two genes for the positions of the two TX antennas and four genes for the antenna positions of the now uncoupled, independent RX antennas. For both optimizations, the best fitness value of every iteration and run was saved and plotted to ensure good convergence of every run. The number of genes has a major impact on the number of generations needed for a fairly good convergence of the optimization solution. This is why for the MIMO array optimization without BMCs fewer iterations are

TABLE IV

INPUT PARAMETERS AND OPTIMIZATION RESULTS FOR TWO EXAMPLES OF GENETICALLY OPTIMIZED MIMO BMAAS AT 76.5 GHz. ONE EXAMPLE CONSISTS OF ONE OPTIMIZATION RESULT EXPLOITING BMCS AND ONE WITH CONVENTIONAL ANTENNAS. THE DIFFERENT BIOMIMETIC PAIRS WITHIN ONE MIMO BMAA ARE MARKED WITH DIFFERENT COLORS

			Genetic Array 1	Genetic Array 2
optimization input parameters		$w_{\mathrm{TX,max}}$	6 cm = 15.30λ	11 cm = 28.05λ
		$w_{\mathrm{RX,max}}$	3 cm = 7.65λ	11 cm = 28.05λ
		$w_{\mathrm{VX,min}}$	7.5 cm = 19.13λ	15 cm = 38.25λ
		η_{max}	5	4
		ξ_{max}	2	2.5
		$d_{\mathrm{b,max}}$	7λ	28λ
		$\mathrm{AF}_{\mathrm{threshold}}$	0.3	0.5
		$N_{\mathrm{iter,max}}$ biom.	1000	2000
		$N_{\mathrm{iter,max}}$ conv.	700	1000
		N_{runs}	30	80
results	**biomimetic BMAAs**	TX Pos. in λ	(0 12.62)	(0 16.32)
		RX Pos. in λ	(0 1.70 6.19 7.49)	(0 1.55 13.31 22.41)
		η	2.6 2.6	1.3 1.0
		ξ	1.4 1.3	0.5 0.2
	conv.	TX Pos. in λ	(0 12.24)	(0 25.37)
		RX Pos. in λ	(0 1.02 5.23 7.65)	(0 7.91 9.82 13.64)

needed, which is, of course, a drawback of the MIMO BMAA design process.

IV. OPTIMIZED MIMO BMAAS AND REALIZATIONS

To show the achievable behavior of the MIMO BMAAs two exemplary, general layouts were introduced in Fig. 4 and their AFs were presented in Figs. 5 and 6 using the values of Table III.

Two exemplary configurations at 76.5 GHz found by the genetic algorithm described in Section III-B.2 are summarized in Table IV. The choice of the input parameters depends highly on the desired application and restrictions. Furthermore, the input values influence how many iterations and runs are favorable and have a high impact on the optimization result.

The first example "Genetic Array 1" is an example of moderate size with a maximum physical aperture of 9 cm. A minimum virtual aperture size of 7.5 cm is set to ensure a maximum BW of the resulting virtual array. The value $d_{\mathrm{b,max}}$ is chosen similar to $w_{\mathrm{RX,max}}$ to make sure that the biomimetically coupled RX antennas are not limited in their possible positions compared to uncoupled RX antennas. This example is conceivable e.g., in an (industry) imaging context where only a limited field of view (FOV) is of interest and multiple targets are present so that the threshold for ambiguities has to be set rather low (here: 0.3). The resulting antenna parameters for the biomimetic and the conventional optimization are listed at the bottom of Table IV. The parameters of the two different BMAA pairs are marked in two distinct colors. Fig. 7 shows the AFs for this example. A genetic optimization using the restrictions listed in Table IV yielded only a very small AFR $= -3.9°, \ldots, 3.9°$ when using conventional antennas without BMCs, see Fig. 7(c). By introducing BMAAs in the

RX array and optimizing the antenna positions and the BMAA parameters, a way broader AFR of $-8.4°, \ldots, 8.4°$ can be reached, cf., Fig. 7(a). It can be seen that by inserting the BMCs the higher correlation values around $\pm\theta_i = \mp\theta_j = 3.9°$ in Fig. 7(c) are significantly reduced for the biomimetic array in Fig. 7(a). When the same antenna placement is considered but the BMCs are omitted, the AFR shrinks to its smallest value of $-3.7°, \ldots, 3.7°$ [Fig. 7(b)] and the grating lobes are significantly higher compared to the result of the conventional genetic optimization of Fig. 7(c). The loss in output power L_{out} for the BMAAs obtained in this example is always less than 10.6 dB for the first BMAA pair, marked in blue in Table IV, and less than 10.4 dB for the second, red-colored BMAA pair.

The second optimization example "Genetic Array 2" is an example with a very large virtual aperture. Because of larger RX and TX aperture sizes with the same antenna position grid, more iterations are needed for good convergence of the optimization. The results for the two optimizations with and without biomimetic coupling are again noted in Table IV. The AFs of the two optimized solutions can be found in Fig. 8. The optimized biomimetic MIMO array in Fig. 8(a) has an AFR of $-12.5°, \ldots, 12.5°$, which is similar, but not equal, to the AFR of the optimized conventional MIMO array of $-14.5°, \ldots, 14.5°$ in Fig. 8(b). However, the MIMO array with optimized BMCs shows the advantage of lower grating lobe levels. This effect can be seen more clearly in the BP of Fig. 8(c). The lobe limiting the AFR is nearly 2 dB lower for the optimized MIMO BMAA. In this example, the BMAA parameters are only moderate and only the first BMAA pair (marked in blue) shows a BMAA characteristic. As a consequence, the normalized output power is only slightly reduced for the two corresponding RX antennas (RX1 and RX2) with $L_{\mathrm{out,min}} = -3.9$ dB.

Incorporating biomimetic coupling to MIMO arrays does not always yield better angular performance for every type of evaluation criterion. The effects of a larger AFR, narrower main beam, lower grating lobes, or lower sidelobe levels (not shown here) are strongly dependent on the number of antennas, the maximum RX and TX apertures, the realizable BMAA parameters, and the optimization parameters. Depending on the restrictions of the array and the achievable behavior without biomimetic coupling, this approach gives more degrees of freedom and different angular behaviors. Therefore, the concept is attractive despite the more complex optimization process and longer optimization time.

To confirm the simulations of the presented AFs the configurations of the deterministic MIMO BMAAs of Table III were fabricated. The antenna arrays were manufactured using a stack of two 127 μm thick RO3003 substrates fused with a Rogers 3001 bonding film. The antenna elements are aperture coupled antennas identical to the ones in [14] and [20]. To implement the biomimetic coupling equivalent scattering parameters were calculated in dependence of the antenna and load impedances and the desired BMAA behavior defined by the parameters η, ξ, and d. The BMCs are then realized by the planar design in form of a folded microstrip line with two open-ended stubs, which was introduced in [14]. The BMCs are optimized in full-wave simulations to meet the desired
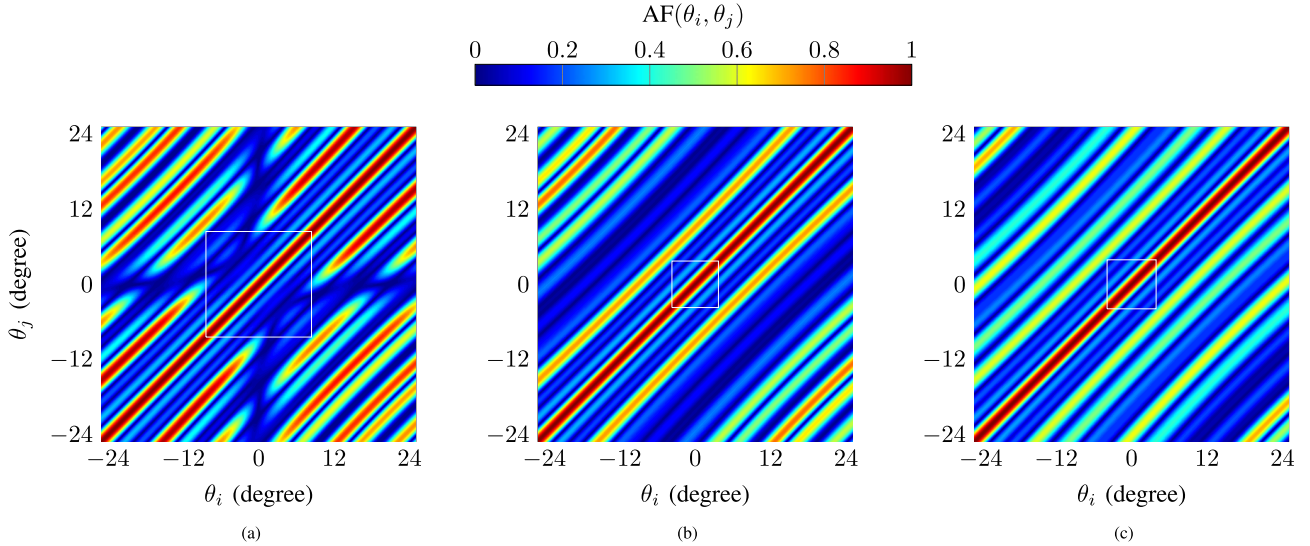
Fig. 7. AFs for the example "Genetic Array 1": (a) optimized array configuration including BMCs in the RX array, (b) same array configuration without BMCs, and (c) independently optimized array without biomimetic coupling applied. Using the same PCB and antenna restrictions, the optimization including BMCs in (a) could yield a much larger AFR (marked by the square) compared to the optimization in (c).
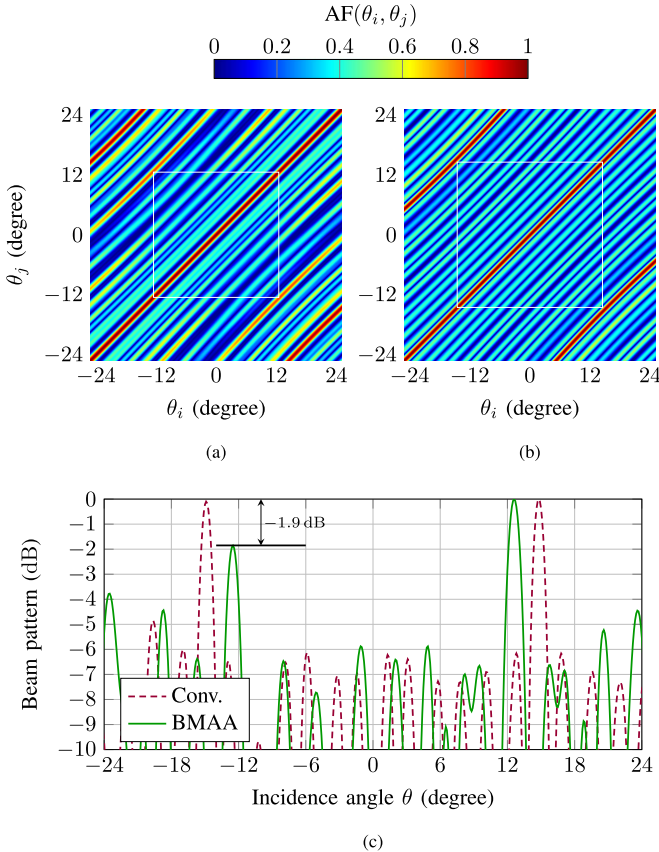

Fig. 8. AFs of the example "Genetic Array 2" for the genetic optimization (a) with and (b) without BMCs and (c) their BP at the angle θ_0 where their first grating lobe occurs (conventional array $\theta_0 = 14.8°$, BMAA $\theta_0 = 12.6°$).

equivalent scattering parameters. A fabricated PCB is shown in Fig. 9. Here, only the waveguide transitions are marked for the antennas, which form the realization of the deterministic MIMO BMAA with smaller BW of Table III.
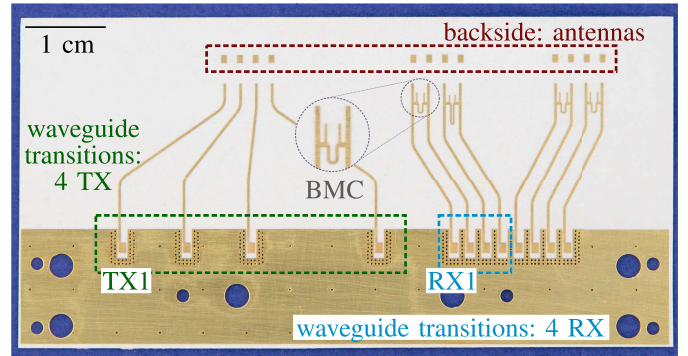

Fig. 9. Antenna board for the deterministic MIMO BMAA with smaller BW of Table III: the patch antennas are located on the backside of the displayed PCB. As there are several RX antennas on this PCB, we marked the waveguide transitions of the respective four RX antennas.

V. RADAR MEASUREMENTS

In this section, we present radar measurements of the MIMO BMAAs. All measurements were carried out in an anechoic chamber. A chirp-sequence frequency modulated radar with interchangeable antenna frontends was used with a carrier frequency of 76.5 GHz and a bandwidth of 2 GHz [35]. Time-division multiplexing (TDM) operation ensures the orthogonality of the TX signals. The recorded signals are evaluated using range-Doppler processing [36], which allows differentiating between multiple targets (as long as they are not in the same range-velocity bin). The steering vectors for each target can be extracted from the respective range-velocity bin in the range-Doppler matrix of every channel.

A. Verification of the AFs and Normalized Output Powers

First, we validate the behavior of the arrays for all angles by measuring the AFs. To do so, one single corner reflector [radar cross section (RCS) = 7 m² at 77 GHz] was positioned in BS direction to the radar at a distance of 4.23 m. The radar itself was mounted on a one-axis turntable with which we recorded the RX and TX steering vectors for an angular range of $\theta = -60°, \ldots, 60°$.
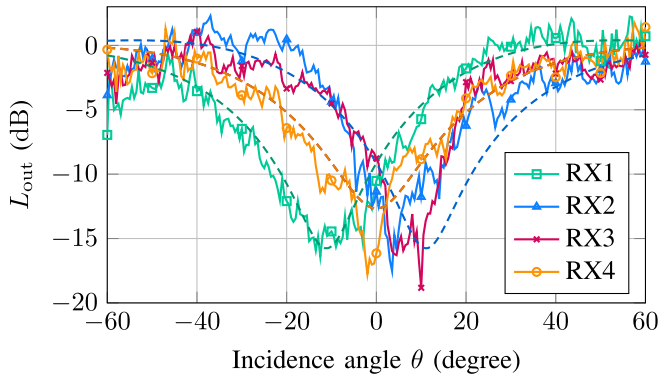
Fig. 10. Measurement (solid lines) and theoretical curves (dashed lines) of L_out for the deterministic array with smaller BW according to Layout B of Fig. 4 and the values of Table III for transmitter TX1. RX1 and RX2 form the off-BS BMAA ($\eta = 1.4$, $\xi = 2.5$) and RX3 and RX4 the BS BMAA ($\eta = 4.3$, $\xi = 0$, theoretical curves overlapping).

Fig. 5(d) depicts the measured AF for the deterministic MIMO BMAA with a larger AFR of Table III. The reduction of the side lobes that leads to the enhancement of the AFR can clearly be seen in the measurement. The simulation in Fig. 5(a) and the measurement in Fig. 5(d) are in very good agreement.

In Fig. 6 the simulated and measured AFs of the deterministic MIMO BMAA with smaller BW of Table III are displayed together with the AFs of its uncoupled board for comparison. The measured AFs in Fig. 6(c) and (d) match well with the simulated AFs in Fig. 6(a) and (b). The AF for the MIMO BMAA in Fig. 6(d) clearly shows a narrower diagonal around BS compared to the array not exploiting biomimetic coupling. A small asymmetry is visible and the effect came out stronger and more focused around BS compared to the simulated AF. The narrower diagonal corresponds to a reduced BW for angles around BS.

The normalized output power measured using the same setup can be seen in Fig. 10. To obtain these curves the output amplitudes of the MIMO BMAA and the uncoupled comparison array were recorded for the target at BS and put in relation to each other. For clarity, we depict the normalized output powers calculated using (3) for only one TX antenna (TX1). All measured L_out curves (solid lines) show the expected behavior of a reduced output power around BS and agree satisfactorily with the theoretical characteristics (dashed lines).

B. Impact on the Angular Resolution

To demonstrate that the observed effects, like the smaller BW of the configuration in Fig. 6, have an impact on the DOA estimation we conducted angular separability measurements. Two different antenna boards were used: the antenna board displayed in Fig. 9 (deterministic MIMO BMAA with smaller BW of Table III) and an identical antenna board on which the BMCs are missing. The radar was mounted on a turntable again. Two cylindrical targets with identical RCS were placed at the same distance to the radar, see Fig. 11. As a consequence, the two targets are in the same range-velocity bin and the signals being reflected by the two targets superimpose.
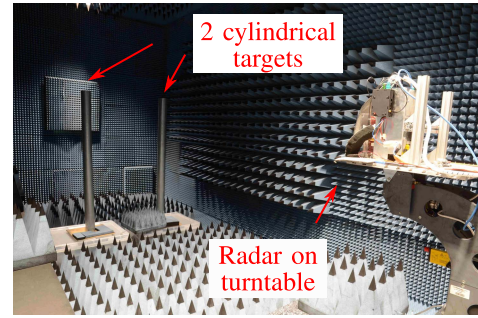

Fig. 11. Two cylindrical targets with identical RCS are arranged symmetrically to the $\theta = 0°$ BS direction of a turntable. The measuring radar is mounted on the turntable.
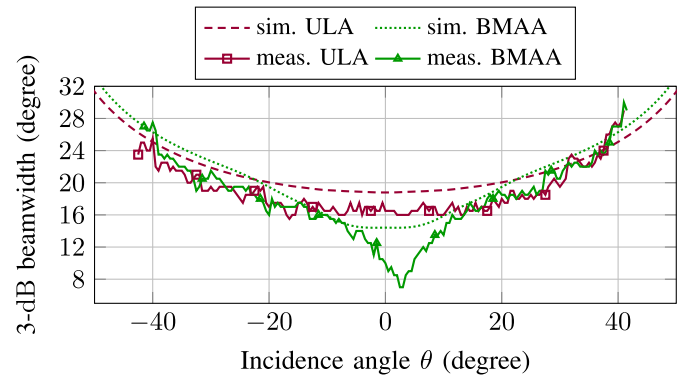

Fig. 12. Simulated and measured 3-dB BW for the deterministic MIMO BMAA with smaller BW of Table III and the identical antenna board without BMCs, corresponding to the AFs in Fig. 6.

The two targets can only be separated in angle, as far as the angular resolution allows it.

Fig. 12 depicts the simulated and measured 3-dB BWs corresponding to the AFs in Fig. 6. The simulated beam is considerably narrower around BS when BMCs are incorporated [cf., Fig. 6(b) versus Fig. 6(a)]. Consequently, the MIMO BMAA yields a better angular resolution for targets in BS direction compared to the uncoupled antenna board. As the angular operating range of increased phase sensitivity of BMAAs is limited around BS (cf., Section II-A), so is the superior angular resolution of the MIMO BMAA. For the MIMO BMAA in Fig. 12 the angular range of improved angular resolution is $\theta = -23°, \ldots, 23°$. For angles $|\theta| \to 90°$ the reduced phase progression slope of the BMAA pairs compared to the conventional phase progression (cf., Fig. 1) leads to a slightly broader 3-dB BW. The measured 3-dB BWs show the expected behavior, with the MIMO BMAA having a smaller BW than in the simulation.

A demonstration that this significant difference in the angular resolution can be seen in measurements is shown in Fig. 13. We evaluated the measured DOAs with a deterministic maximum likelihood angle estimation approach [37], [38] using the complex, un-normalized steering vectors. When the two targets are placed 30° or 20° apart, both the MIMO array consisting of conventional ULAs and the deterministic MIMO BMAA can resolve the two targets, cf., Fig. 13(a) and (b). Because of misalignment, small deviations from the theoretical
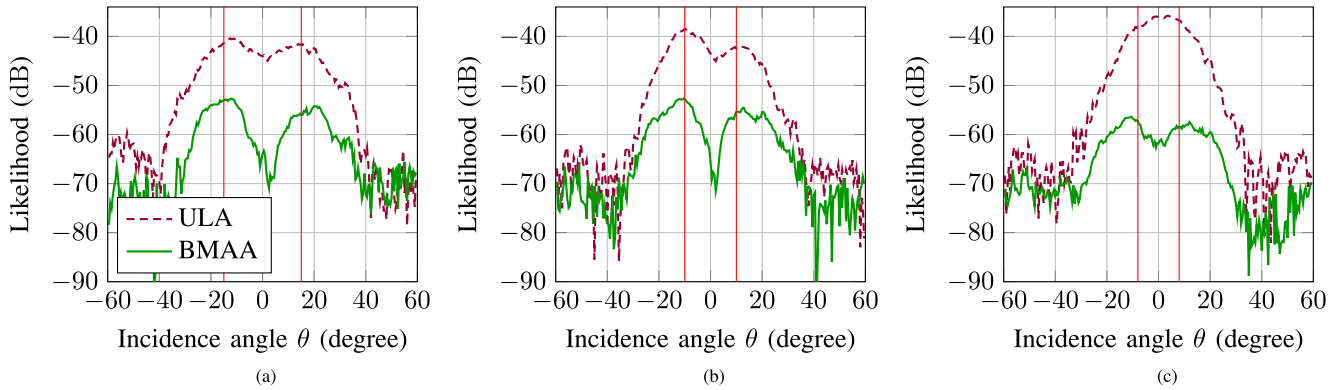
Fig. 13. Measured, un-normalized likelihood for two targets in the same range-velocity bin for the deterministic MIMO BMAA with smaller BW of Table III (———) and the identical array without BMCs but the same antenna positions (-----). The targets are positioned symmetrically around BS and their true DOA is indicated with red lines. (a) 2 targets at $\pm15°$. (b) 2 targets at $\pm10°$. (c) 2 targets at $\pm8°$.

DOA are possible, but the scenario is always identical for both arrays. The MIMO BMAA shows a better target separability compared to the conventional ULA design. In contrast to the conventional MIMO array without BMCs, a clear notch between the likelihood lobes is visible for both measurements, when considering the MIMO BMAA. For an even smaller target separation of $\Delta\theta = 16°$ in Fig. 13(c), the ULA array is not capable to resolve the two targets anymore. However, the MIMO BMAA still allows differentiating between two likelihood lobes and thus, between two targets. Because of the reduced output power (cf., Fig. 10), the MIMO BMAA has a lower SNR within the angular spectra compared to the conventional MIMO array. The noise levels in Fig. 13 are similar for both arrays. Despite the reduced SNR in the angular spectra the biomimetically coupled array shows a superior angular separability compared to the uncoupled array. But of course, the targets have to be detectable. It should be noted that potential correlation of the output signals can influence the DOA estimation using the maximum likelihood approach. Furthermore, the angle-dependent behavior of the biomimetic coupling may lead to an angle-dependent influence on the noise. Thus, it is a question for future research how and if biomimetic coupling is linked to correlated signals and noise shaping and how these points affect the angle estimation.

VI. Conclusion

In this article, it has been shown that the special phase progression for BMAAs can be translated to an angle-dependent antenna spacing of the biomimetically coupled antennas. This new way of modeling BMAAs was introduced as the effective biomimetic antenna distance. When including pairwise biomimetically coupled antennas in the RX array of a MIMO antenna configuration, the RX antennas seem to move with respect to the azimuth angle of a radar target. As a consequence, the angular behavior of the MIMO array is changed significantly, new degrees of freedom arise for array synthesis and the DOA estimation capabilities of MIMO radars can be improved considerably. A genetic algorithm was proposed and adapted as an efficient manner to design such a MIMO BMAA. It was demonstrated by simulations and measurements that the AFR for the DOA estimation can be enlarged significantly,

grating lobe levels can be reduced or the beamwidth of the array can be reduced compared to a conventional antenna board occupying the same physical aperture. Because of the reduced beamwidth an improved angular resolution can be achieved.

References

[1] D. Zankl, S. Schuster, R. Feger, and A. Stelzer, "What a blast!: A massive MIMO radar system for monitoring the surface in steel industry blast furnaces," *IEEE Microw. Mag.*, vol. 18, no. 6, pp. 52–69, Sep. 2017.

[2] S. Sun, A. P. Petropulu, and H. V. Poor, "MIMO radar for advanced driver-assistance systems and autonomous driving: Advantages and challenges," *IEEE Signal Process. Mag.*, vol. 37, no. 4, pp. 98–117, Jul. 2020.

[3] M. Zlatanski, P. Sommer, F. Zurfluh, and G. L. Madonna, "Radar sensor for fenceless machine guarding and collaborative robotics," in *Proc. IEEE Int. Conf. Intell. Saf. Robot. (ISR)*, Aug. 2018, pp. 19–25.

[4] Z. Zhang, Y. Zhao, and J. Huang, "Array optimization for MIMO radar by genetic algorithms," in *Proc. 2nd Int. Congr. Image Signal Process. (CISP)*, Oct. 2009, pp. 1–4.

[5] P. Uthansakul, D. Assanuk, and M. Uthansakul, "The use of genetic algorithm for designing MIMO antenna placement," in *Proc. Int. Conf. Comput. Inf. Appl.*, Dec. 2010, pp. 414–417.

[6] A. Sayin, E. G. Hoare, and M. Antoniou, "Design and verification of reduced redundancy ultrasonic MIMO arrays using simulated annealing & genetic algorithms," *IEEE Sensors J.*, vol. 20, no. 9, pp. 4968–4975, May 2020.

[7] C. Vasanelli, R. Batra, and C. Waldschmidt, "Optimization of a MIMO radar antenna system for automotive applications," in *Proc. 11th Eur. Conf. Antennas Propag. (EUCAP)*, Mar. 2017, pp. 1113–1117.

[8] A. Di Serio, P. Hügler, F. Roos, and C. Waldschmidt, "2-D MIMO radar: A method for array performance assessment and design of a planar antenna array," *IEEE Trans. Antennas Propag.*, vol. 68, no. 6, pp. 4604–4616, Jun. 2020.

[9] R. N. Miles, D. Robert, and R. R. Hoy, "Mechanically coupled ears for directional hearing in the parasitoid fly ormia ochracea," *J. Acoust. Soc. Amer.*, vol. 98, no. 6, pp. 3059–3070, Dec. 1995.

[10] A. R. Masoumi, Y. Yusuf, and N. Behdad, "Biomimetic antenna arrays based on the directional hearing mechanism of the parasitoid fly Ormia Ochracea," *IEEE Trans. Antennas Propag.*, vol. 61, no. 5, pp. 2500–2510, May 2013.

[11] P. Grüner, T. Chaloun, and C. Waldschmidt, "Enhanced angle estimation accuracy of ultra compact radars inspired by a biomimetic approach," in *IEEE MTT-S Int. Microw. Symp. Dig.*, Jun. 2017, pp. 1425–1428.

[12] R. J. Kozick, F. T. Dagefu, and B. M. Sadler, "Two-element biomimetic antenna array design and performance," in *Proc. IEEE Int. Conf. Acoust., Speech Signal Process. (ICASSP)*, May 2020, pp. 4747–4751.

[13] P. Grüner, M. Geiger, and C. Waldschmidt, "Ultracompact monostatic MIMO radar with nonredundant aperture," *IEEE Trans. Microw. Theory Techn.*, vol. 68, no. 11, pp. 4805–4813, Nov. 2020.

[14] P. Grüner, I. Dorsch, and C. Waldschmidt, "N-element biomimetic antenna arrays," *IEEE Trans. Antennas Propag.*, vol. 69, no. 7, pp. 3899–3912, Jul. 2021.

[15] M. Akçakaya and A. Nehorai, "Biologically inspired coupled antenna beampattern design," *Bioinspir. Biomim.*, vol. 5, no. 4, Art. no. 046003, pp. 1–11, Nov. 2010.

[16] A. M. Elfrgani and R. G. Rojas, "Biomimetic antenna array using non-foster network to enhance directional sensitivity over broad frequency band," *IEEE Trans. Antennas Propag.*, vol. 64, no. 10, pp. 4297–4305, Oct. 2016.

[17] M. R. Nikkhah, M. A. Panahi, H. Luyen, N. Behdad, and H. R. Bahrami, "Capacity enhancement of MIMO systems using electrically-small, biomimetic antenna arrays," in *Proc. Int. Workshop Antenna Technol. (iWAT)*, Mar. 2018, pp. 1–3.

[18] A. R. Masoumi, K. Ghaemi, and N. Behdad, "A two-element bio-mimetic antenna array with enhanced angular resolution and optimized power extraction," *IEEE Trans. Antennas Propag.*, vol. 63, no. 3, pp. 1059–1066, Mar. 2015.

[19] Y. Zang, H. Luyen, H. R. Bahrami, and N. Behdad, "An analytic synthesis method for two-element biomimetic antenna arrays," *IEEE Trans. Antennas Propag.*, vol. 68, no. 4, pp. 2797–2809, Apr. 2020.

[20] P. Grüner, T. Chaloun, and C. Waldschmidt, "A generalized model for two-element biomimetic antenna arrays," *IEEE Trans. Antennas Propag.*, vol. 67, no. 3, pp. 1630–1639, Mar. 2019.

[21] E. Mohammadi, B. Behzadnezhad, and N. Behdad, "An angle-sensing infrared detector using a two-element biomimetic antenna array," *IEEE Trans. Antennas Propag.*, vol. 66, no. 11, pp. 5818–5826, Nov. 2018.

[22] A. R. Masoumi and N. Behdad, "Architecture, design, and nonlinear optimization of three-element biomimetic antenna arrays," *IEEE Antennas Wireless Propag. Lett.*, vol. 12, pp. 1416–1419, Dec. 2013.

[23] P. Grüner, M. Klose, and C. Waldschmidt, "A radar system concept for 2D unambiguous angle estimation using widely spaced MMICs with antennas on-chip at 150 GHz," in *IEEE MTT-S Int. Microw. Symp. Dig.*, Aug. 2020, pp. 1279–1282.

[24] F. T. Dagefu, J. Oh, and K. Sarabandi, "A sub-wavelength RF source tracking system for GPS-denied environments," *IEEE Trans. Antennas Propag.*, vol. 61, no. 4, pp. 2252–2262, Apr. 2013.

[25] M. R. Nikkhah, K. Ghaemi, and N. Behdad, "A three-element bio-mimetic antenna array with an electrically small triangular lattice," *IEEE Trans. Antennas Propag.*, vol. 65, no. 8, pp. 4007–4016, Aug. 2017.

[26] A. Jelodar, M. Soleimani, and S. H. Sedighy, "Biologically inspired four elements compact antenna arrays with enhanced sensitivity for direction of arrival estimation," *Iran. J. Elec. Electron. Eng.*, vol. 16, no. 2, pp. 130–136, Jun. 2020.

[27] P. Grüner, S. Nguyen, T. Chaloun, and C. Waldschmidt, "Enhancing angle estimation for off-boresight targets using biomimetic antenna arrays," in *Proc. 15th Eur. Radar Conf. (EuRAD)*, Sep. 2018, pp. 1377–1380.

[28] A. R. Masoumi and N. Behdad, "An improved architecture for two-element biomimetic antenna arrays," *IEEE Trans. Antennas Propag.*, vol. 61, no. 12, pp. 6224–6228, Dec. 2013.

[29] R. J. Kozick, F. T. Dagefu, and B. M. Sadler, "Two-element biomimetic antenna array for power extraction / phase amplification tradeoff," in *Proc. 14th Eur. Conf. Antennas Propag. (EuCAP)*, Mar. 2020, pp. 1–5.

[30] C. Vasanelli, R. Batra, A. Di Serio, F. Bögelsack, and C. Waldschmidt, "Assessment of a millimeter-wave antenna system for MIMO radar applications," *IEEE Antennas Wireless Propag. Lett.*, vol. 16, pp. 1261–1264, 2017.

[31] M. Eric, A. Zejak, and M. Obradovic, "Ambiguity characterization of arbitrary antenna array: Type I ambiguity," in *Proc. IEEE 5th Int. Symp. Spread Spectr. Techn. Appl.*, vol. 2, Sep. 1998, pp. 399–403.

[32] I. Bekkerman and J. Tabrikian, "Target detection and localization using MIMO radars and sonars," *IEEE Trans. Signal Process.*, vol. 54, no. 10, pp. 3873–3883, Oct. 2006.

[33] J. H. Holland, *Adaptation in Natural and Artificial Systems: An Introductory Analysis With Applications to Biology, Control, and Artificial Intelligence*. Cambridge, MA, USA: MIT Press, 1992.

[34] R. L. Haupt, "An introduction to genetic algorithms for electromagnetics," *IEEE Antennas Propag. Mag.*, vol. 37, no. 2, pp. 7–15, Apr. 1995.

[35] P. Hügler, F. Roos, M. Schartel, M. Geiger, and C. Waldschmidt, "Radar taking off: New capabilities for UAVs," *IEEE Microw. Mag.*, vol. 19, no. 7, pp. 43–53, Nov. 2018.

[36] V. Winkler, "Range Doppler detection for automotive FMCW radars," in *Proc. Eur. Microw. Conf.*, Oct. 2007, pp. 166–169.

[37] H. Krim and M. Viberg, "Two decades of array signal processing research: The parametric approach," *IEEE Signal Process. Mag.*, vol. 13, no. 4, pp. 67–94, Jul. 1996.

[38] C. Vasanelli *et al.*, "Calibration and direction-of-arrival estimation of millimeter-wave radars: A practical introduction," *IEEE Antennas Propag. Mag.*, vol. 62, no. 6, pp. 34–45, Dec. 2020.

Ines Dorsch received the M.Sc. degree in electrical engineering from Ulm University, Ulm, Germany, in 2019, where she is currently pursuing the Ph.D. degree at the Institute of Microwave Engineering.

Her current research interests include biomimetic antenna systems in the microwave and millimeter-wave range and their applications in sensor networks.

Ms. Dorsch was a recipient of the ARGUS Science Award in 2019.

Patrik Grüner (Member, IEEE) received the M.Sc. degree in electrical engineering from Ulm University, Ulm, Germany, in 2015, where he is currently pursuing the Ph.D. degree.

In 2015, he joined the Institute of Microwave Engineering (MWT), Ulm University. His current research interests include compact frequency-modulated continuous wave (FMCW) radar sensors and biomimetic antenna systems both in the microwave and millimeter-wave range.

Mr. Grüner was a recipient of the ARGUS Science Award in 2013 and the Best Paper Award of the 2013 International Workshop on Antenna Technology.

Markus Klose received the M.Sc. degree in electrical engineering from Ulm University, Ulm, Germany, in 2019. In his master's thesis at the Institute of Microwave Engineering, Ulm University, he did research on an multiple-input multiple-output (MIMO)-radar system utilizing biomimetic antennas for 2-D angle estimation.

In 2020, he joined Astyx GmbH (Cruise Munich), Ottobrunn, Germany, where he is currently working as a Hardware Engineer for radar systems.

David Schmucker received the M.Sc. degree in electrical engineering from Ulm University, Ulm, Germany, in 2020.

In 2020, he joined Tesat Spacecom, Backnang, Germany, where he is currently working as a Rx/Tx System Developer.

Christian Waldschmidt (Senior Member, IEEE) received the Dipl.-Ing. (M.S.E.E.) and Dr.-Ing. (Ph.D.E.E.) degrees from University Karlsruhe (TH), Karlsruhe, Germany, in 2001 and 2004, respectively.

From 2001 to 2004, he was a Research Assistant with the Institut für Höchstfrequenztechnik and Elektronik (IHE), Universität Karlsruhe (TH). Since 2004, he has been with Robert Bosch GmbH, Stuttgart, Germany, in the business units Corporate Research and Chassis Systems. He was heading different research and development teams in microwave engineering, RF-sensing, and automotive radar. In 2013, he returned to academia. He was appointed as the Director of the Institute of Microwave Engineering, Ulm University, Ulm, Germany, as a Full Professor. He authored or coauthored more than 200 scientific publications and more than 20 patents. The research topics focus on radar and RF-sensing, millimeter-wave and submillimeter-wave engineering, antennas and antenna arrays, RF and array signal processing.

Mr. Waldschmidt is member of the Executive Committee Board of the German MTT/AP joint chapter and member of the German Information Technology Society (ITG). He was a co-recipient of 11 best paper awards since 2014. He served as the Chair of the IEEE MTT-27 Technical Committee on wireless enabled automotive and vehicular applications. He was a two-time TPC Chair and the General Chair of the IEEE MTT International Conference on Microwaves for Intelligent Mobility. Since 2018, he serves as an Associate Editor for the IEEE MTT MICROWAVE WIRELESS COMPONENTS LETTERS (MWCL). He is a Reviewer for multiple IEEE transactions and many IEEE conferences in the field of microwaves.